Entropic Self-Assembly of Diblock Copolymers into Disordered and Ordered Micellar Phases[†]

Barbara Capone,*[,‡] Carlo Pierleoni,[§] Jean-Pierre Hansen,[‡] and Vincent Krakoviack[⊥]

University Chemical Laboratory, Lensfield Road, Cambridge CB2 1EW, United Kingdom, CNISM and Physics Department, University of L'Aquila, I-67010 L'Aquila, Italy, and Laboratoire de Chimie, École Normale Supérieure de Lyon, 69364 Lyon Cedex 07, France

Received: July 6, 2008; Revised Manuscript Received: August 22, 2008

We investigate the self-assembly of an athermal model of AB diblock copolymers into disordered and ordered micellar microphases. The original microscopic lattice model with ideal A strands and self-avoiding B strands is mapped onto a system of ultrasoft dumbbells, with monomer-averaged effective interactions between the centers of mass (CMs) of the two blocks. Extensive Monte Carlo simulations of this coarse-grained model are reported for several length ratios $f = L_A/(L_A + L_B)$ of the two strands of lengths L_A and L_B. Clear-cut evidence is found for clustering and self-assembly into micelles with a mean aggregation number of $\bar{n} \simeq 100$ beyond a critical micellar concentration (cmc) in the semidilute regime. The cmc is found to decrease with increasing f, as predicted by an analytic calculation based on the random phase approximation. The initially disordered dispersion of polydisperse spherical micelles undergoes a disorder−order transition to a micellar crystal phase at higher copolymer concentrations. The effective pair potential between the micellar CMs is determined by inverting the measured CM−CM pair distribution function and is found to become steeper with increasing density.

I. Introduction

Self-assembly and microphase separation of large molecules with dual physical or chemical functionalities are ubiquitous phenomena in complex fluids or soft matter, with far-reaching consequences in materials science or molecular and cell biology. One of the best-known examples is the formation of micelles, vesicles, microemulsions, and bilayer membranes in solutions of amphiphilic or surfactant molecules formed of a hydrophilic polar head group and one or several hydrophobic tails.[1] Similarly, AB diblock copolymers in solution self-assemble into a wide variety of microphases, including lamellar, hexagonal, cubic, or bicontinuous phases.[2] While microphase separation in copolymer melts is well understood within self-consistent mean field theory[3,4] and its improvements,[5,6] the theoretical understanding of self-assembly in copolymer solutions is much less advanced[7] mainly because polymers in solution no longer obey ideal (Gaussian) statistics and because the osmotic compressibility can be large, as opposed to the usual incompressibility assumption for melts. Monte Carlo (MC) simulations of copolymer solutions have so far been restricted to short copolymer chains.[8−10]

Self-assembly and microphase separation generally arise from a competition between entropic (which opposes self-assembly) and enthalpic (which favors self-assembly) contributions to the total free energy. This competition, controlled by the temperature and the polymer concentration, leads to the very rich phase diagrams observed for various copolymers in selective solvent.[2,11] For instance, the complex phase diagrams of styrene−isoprene diblock copolymers in various solvents have been mapped out experimentally in great detail by varying temperature, concentration, solvent selectivity, as well as the relative sizes of the two blocks by a combination of light scattering, small-angle neutron and X-ray diffraction, and rheological studies.[12,13] In view of the large number of independent physical parameters involved, a fully "first principles" theoretical description of such complex behavior is clearly out of reach. For that reason, we focus in this paper on a highly simplified copolymer model in the hope of gaining insight into generic phase behavior controlled by a small number of variables. The model which is investigated is athermal, that is, its phase behavior is entropy-driven, so that it is independent of temperature and is controlled only by polymer concentration and the relative sizes of the two blocks. Our copolymer model is reminiscent of an athermal model introduced some time ago by Bolhuis and Frenkel to investigate entropic micellization of a crude model of surfactant solutions,[14] but the much larger size of copolymer macromolecules allows an implicit representation of the selective solvent in the present case. Despite the drastic simplification, monomer-level simulations of long copolymer chains would still be computationally extremely demanding, and we have therefore resorted to a systematic coarse-graining strategy which has proved very successful for the description of dilute and semidilute homopolymer solutions[15−17] and of polymer−colloid mixtures.[18,19]

Within this strategy, polymers are represented by one or several soft effective particles (referred to as blobs), and effective interactions between the centers of mass (CMs) of these blobs are calculated by averaging over monomer degrees of freedom.[20−22] In the case of diblock copolymers, the minimal representation involves two such blobs, which are tethered by an entropic spring. This strategy leads to a reduction of the computational effort in MC simulations by orders of magnitude, allowing the observation of copolymer clustering, microphase separation, and micelle ordering within reasonable computer times. The coarse-grained representation of copolymers also lends itself to the

[†] Part of the "PGG (Pierre-Gilles de Gennes) Memorial Issue".
* To whom correspondence should be addressed.
[‡] University Chemical Laboratory.
[§] University of L'Aquila.
[⊥] École Normale Supérieure de Lyon.

10.1021/jp805946z CCC: $40.75
Published on Web 11/19/2008

application of standard theoretical approaches, like the random phase approximation (RPA).

The picture of diblock copolymers as soft colloidal dumbbells has also been considered recently by other authors. Thus, using a direct extension of our theoretical coarse-graining strategy for homopolymers based on the polymer reference interaction site model (PRISM) theory[23] and a simple analytic theory for the microscopic monomer correlations in diblock copolymers, Sambriski and Guenza have explored how the correlations at the monomer level are reflected at the mesoscale by computing the pair distribution functions of the block CMs in the weak segregation regime.[24] Good agreement with simulation results was found. Along another line of approach, Eurich et al. have developed a so-called disphere model for block copolymers[25] by extending the Gaussian version[26] of the soft-ellipsoid model of Murat and Kremer[27] to the case of diblocks. Using this model, they could successfully study structural and dynamical properties in the bulk and in various thin film geometries.

A preliminary account of parts of the present work, restricted to the case of equal length copolymer blocks, has been reported elsewhere.[28]

II. The Model

We consider solutions of N AB diblock copolymers in a volume V, so that the mean polymer density is $\rho = N/V$. The A and B strands are linear chains of M_A and M_B monomers, the last monomer of A coinciding with the first monomer of B (the two strands are tethered at this common monomer). In the underlying microscopic model, the monomers are placed on a cubic lattice of spacing b, such that the lengths of the two strands are $L_A = (M_A - 1)b$ and $L_B = (M_B - 1)b$; b will henceforth be taken as the unit of length. The relative length of the two strands is characterized by the ratio

$$f = \frac{L_A}{L_A + L_B} \tag{1}$$

The microscopic model is defined by the three monomer−monomer couplings AA, AB, and BB. In the simple athermal ISS model introduced in ref 28, the A strands are ideal (I); the B strands are self (S) and mutually avoiding, that is, each site can accommodate at most one B monomer; the A and B strands are mutually avoiding (loosely referred to as S), that is, no pair of A and B monomers can occupy the same site. Self-avoiding walk (SAW) statistics account for excluded volume effects and correspond to good solvent conditions. Ideal statistics approximately mimic θ-solvent conditions. In other words, the selective solvent acts as a good solvent for the B strands and as a θ-solvent for the A strands, while AB pairs behave as that in good solvent. This very simple model is athermal. There is no enthalpic contribution as would result, for example, from an attraction of $-\epsilon$ between nonbonded adjacent monomers. For given total length $L = L_A + L_B$ and f, the only thermodynamic variable is the polymer density, or concentration, ρ. In the low-density limit, the two strands have radii of gyration of $R_{gA} \sim L_A^{1/2}$ and $R_{gB} \sim L_A^{\nu}$ (with the exponent $\nu \simeq 0.588$[29] close to the Flory value 3/5[30]). The total radius of gyration of an isolated diblock copolymer is R_g, roughly (but not exactly) equal to $(R_{gA}^2 + R_{gB}^2)^{1/2}$. R_g defines the overlap concentration of the copolymers

$$\rho^* = \frac{3}{4\pi R_g^3} \tag{2}$$

and a convenient density variable is ρ/ρ^*; $\rho/\rho^* \ll 1$ corresponds to the dilute solution regime, while the semidilute regime is for $\rho/\rho^* \gtrsim 1$.

Full monomer-level MC simulations of the ISS model would be computationally extremely demanding for long chains ($L \gg 1$) and the large numbers of copolymers ($N \gg 1$) required to explore clustering, self-assembly, and microphase separation. For that reason, we have adopted a systematic coarse-graining strategy inspired by earlier work on binary homopolymer mixtures[22,31,32] and on the related ISI diblock copolymer model, which self-assembles into a lamellar phase beyond a critical density.[33] Within this reductionist approach, each diblock copolymer is mapped onto a "soft dumbbell", whereby A and B blocks are each represented by a single effective particle or blob, centered on the block CM. The CMs of the two blobs of a given copolymer are tethered by an anharmonic entropic spring. The effective interactions between tethered and untethered A and B blobs are obtained by averaging over monomer conformations of a pair of AB copolymers, as explained in the following section. While our preliminary investigation[28] was restricted to the symmetric case $f = 1/2$, the present investigation examines the influence of the size ratio (eq 1) on the phase behavior by exploring asymmetric copolymers with $f = 0.8$, 0.6, 0.4, and 0.2.

III. Effective Interactions

The "soft dumbbell" representation of the AB diblock copolymer model requires the knowledge of three effective intermolecular pair potentials $v_{AA}(r)$, $v_{AB}(r)$, and $v_{BB}(r)$ and one effective intramolecular pair potential $\Psi_{AB}(r)$, as functions of the CM−CM distance r. It proves very instructive to consider in parallel the binary mixture obtained by cutting each copolymer into separate A and B homopolymers; this mixture is characterized by three effective intermolecular pair potentials which are, a priori, different from their copolymer counterparts, while $\Psi_{AB}(r) \equiv 0$. We have determined the effective pair potentials in the low-density limit ($\rho \to 0$) by carrying out MC simulations of the underlying full monomer model of isolated pairs of AB copolymers and that of A−A, A−B, and B−B homopolymer pairs. In the latter case, separate MC simulations are carried out for each of the three $\alpha\beta$ pairs, and the CM−CM pair distribution functions $g_{\alpha\beta}(r)$ are computed by averaging over monomer conformations for fixed CM−CM distances r. The effective pair potentials, which coincide in the $\rho \to 0$ limit with the potentials of mean force, are then given by

$$v_{\alpha\beta}(r) = -k_B T \ln g_{\alpha\beta}(r) \tag{3}$$

In the case of AB copolymers, the intramolecular potential $\Psi_{AB}(r)$ is determined by MC simulations of a single copolymer. The intramolecular CM−CM distribution function $s_{AB}(r)$ is then determined by averaging again over monomer conformations of the tethered A and B blocks, and $\Psi_{AB}(r)$ then follows from

$$\Psi_{AB}(r) = -k_B T \ln s_{AB}(r) \tag{4}$$

Calculation of the intermolecular copolymer pair potentials requires MC simulations of a pair of AB copolymers to determine the three partial distribution functions $g_{\alpha\beta}(r)$, given the intramolecular distribution $s_{AB}(r)$; the inversion is less straightforward because one is faced with a four-body (four blob) problem. An exact set of equations relating the $g_{\alpha\beta}(r)$ to the $v_{\alpha\beta}(r)$ for given $s_{AB}(r)$ has been derived by B. M. Ladanyi and

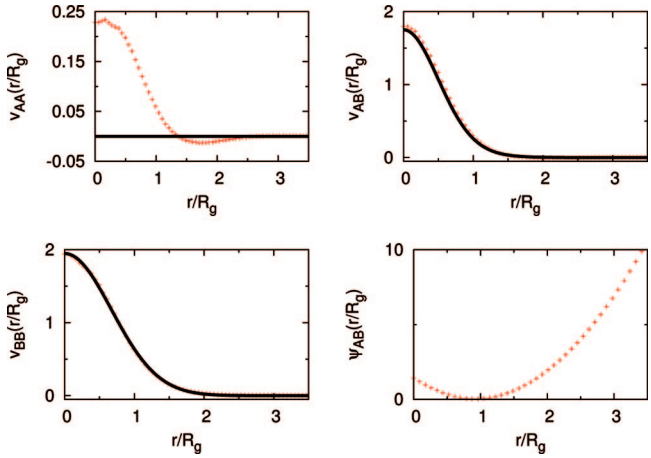

Figure 1. Effective blob−blob interaction potentials $v_{\alpha\beta}(r)$ in units of k_BT as functions of the CM−CM distance r normalized by the radius of gyration R_g, from low-density MC simulations, for $f = 0.4$. Crosses: AB diblock copolymers; full curves: binary A/B mixture. The lower right curve is the AB diblock tethering potential $\Psi_{AB}(r)$.

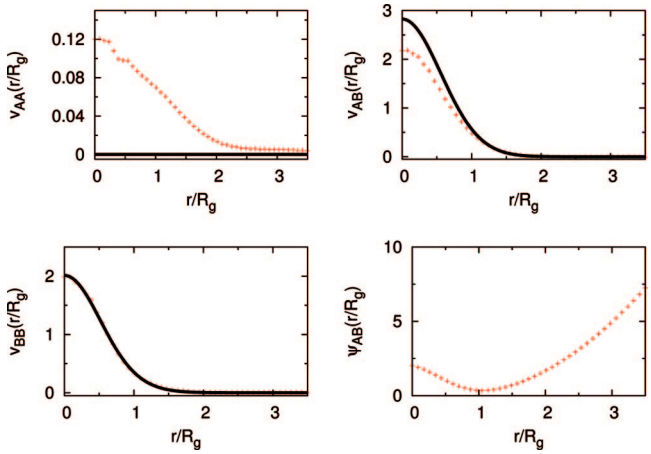

Figure 2. Same as Figure 1 but for $f = 0.8$.

D. Chandler in the context of diatomic molecules.[34] Details of the numerical procedure to solve these equations for the $v_{\alpha\beta}(r)$ in the copolymer case are given in ref 33 and summarized in Appendix A.

Results for size ratios $f = 0.4$ and 0.8 are shown in Figures 1 and 2, where the effective intermolecular and intramolecular potentials for ISS diblock copolymers are compared to the corresponding effective potentials for ISS binary mixtures.

Results for the symmetric case $f = 1/2$ are shown in Figure 1 of ref 28, while results obtained for $f = 0.2$ and 0.6 are not reported here but show similar trends.

In all cases, $v_{AB}(r)$ and $v_{BB}(r)$ are roughly Gaussian with an amplitude at full overlap ($r = 0$) on the order of $2k_BT$. The key finding is that these effective potentials are very similar for block copolymers and binary homopolymer mixtures, especially so for nearly symmetric situations ($f = 0.4-0.6$). The $v_{AA}(r)$ is strictly zero in the case of the binary mixture since the A chains are ideal. In the case of diblock copolymers, $v_{AA}(r)$ is nonzero due to the tethering to SAW B blocks, which induce a weak repulsion on the order of $0.2k_BT$ at full overlap in the symmetric case. This repulsion decreases as f increases due to the weaker influence of the shorter B blocks. In the opposite case of short A strands, $f = 0.2$, $v_{AA}(r = 0)$ reaches an amplitude of $0.4k_BT$, still much smaller than $v_{BB}(r = 0)$. If a simple Gaussian

$$v_{\alpha\beta}(r) = A_{\alpha\beta} \exp[-a_{\alpha\beta}(r/R_g)^2] \quad (5)$$

is fitted to the simulation data, the width parameter $a_{\alpha\beta}$ is consistently close to 1 (cf. Table 1), that is the range of the effective pair potentials $v_{\alpha\beta}(r)$ is close to the radius of gyration of the copolymer (or of $R_g = (R_{g\alpha}^2 + R_{g\beta}^2)^{1/2}$ in the case of a binary mixture of homopolymers) as one would expect.

The effective intramolecular (or tethering) potential $\Psi_{AB}(r)$ may be expected to be the superposition of the intermolecular potential $v_{AB}(r)$ at short distances (when the blobs associated with the A and B blocks strongly overlap) and a parabolic potential at larger distances, similar to the harmonic entropic spring of a Gaussian chain, albeit with a renormalized spring constant

$$\Psi_{AB}(r) \simeq v_{AB}(r) + \frac{k}{2}\left(\frac{r - r_0}{R_g}\right)^2 + c \quad (6)$$

This expectation is borne out by the MC simulations; values of k and r_0/R_g are listed in Table 1.

The effective potentials shown here are extracted from MC data for a total length $L = L_A + L_B = 500$. Runs carried out for longer chains ($L = 1000$ and 2000) do not indicate a significant L dependence as one might expect from earlier results for homopolymers,[15] although a finite size scaling analysis in that case points to differences in the amplitudes $A_{\alpha\beta}$ on the order of 5% between $L = 500$ and the scaling limit $L \to \infty$.[35]

It is important to stress at this stage that the effective potentials derived here are strictly valid in the low-density limit but will be used throughout this paper to explore copolymer clustering and self-assembly, which will be shown to occur in the semidilute regime. From earlier experience with effective interactions between homopolymers, we know that effective interactions depend significantly (but not dramatically) on polymer density when $\rho/\rho^* \gtrsim 1$.[15] We have chosen to ignore this density dependence of the $v_{\alpha\beta}(r)$ in this paper partly for reasons of clarity and simplicity and partly because the inversion procedure from finite density $g_{\alpha\beta}(r)$ data would be very laborious in the case of diblock copolymers. We will return to this important point in the conclusion.

We have made a second simplifying assumption, namely, that $v_{AA}(r) = 0$ for diblock copolymers, as would be exactly the case for a binary mixture. This is not unreasonable since $v_{AA}(r = 0)$ is only about 10% of $v_{AB}(r = 0)$ and $v_{BB}(r = 0)$, as shown in Figures 1 and 2. To be consistent, we have used the binary mixture intermolecular blob−blob potentials, with parameters listed in Table 1, together with the intramolecular potential (eq 6) in all of our calculations. We have checked that this simplified force field leads to small quantitative differences but not to qualitatively different results compared to data obtained within the full two-blob representation, as expected from the great similarity of the effective potentials, as illustrated in Figures 1 and 2.

IV. RPA Estimate of the Clustering Density

The weakness of the effective blob−blob interactions $v_{\alpha\beta}(r)$ relative to k_BT and their softness allow the application of standard approximations of statistical mechanics to the soft dumbbell representation of diblock copolymers. Thus, the RPA, which has been shown to yield quantitatively accurate predictions for homopolymers[31] and for the clustering of penetrable particles,[36−38] is easily generalized to soft dumbbells. If $\underline{S}(k)$ is

TABLE 1: Paramenters of Effective Blob−Blob Pair Potentials (eqs 5 and 6)[a]

f	A_{AA}/k_BT	A_{AB}/k_BT	A_{BB}/k_BT	a_{AA}	a_{AB}	a_{BB}	$k/(2k_BT)$	r_0/R_g
				Diblock				
1/5	0.40	1.08	1.97	2.16	1.79	0.98	1.44	0.78
2/5	0.25	1.81	1.95	1.41	1.82	1.11	1.57	0.91
3/5	0.16	2.52	1.90	0.98	1.74	1.26	1.53	1.07
4/5	0.11	2.19	2.00	0.51	1.52	1.76	1.08	1.01
f	A_{AA}/k_BT	A_{AB}/k_BT	A_{BB}/k_BT	a_{AA}	a_{AB}	a_{BB}		
				Binary Mixture				
1/5	0.0	0.92	1.97	0.0	1.87	0.98		
2/5	0.0	1.74	1.95	0.0	1.94	1.11		
3/5	0.0	2.61	1.90	0.0	1.85	1.26		
4/5	0.0	2.82	1.99	0.0	1.61	1.76		

[a] Diblock: parameters determined from MC data for a pair of AB copolymers. Binary mixture: parameters for the A−B binary mixture.

the 2 × 2 matrix of partial blob−blob structure factors $S_{\alpha\beta}(k)$, $\underline{S_0}(k)$ is the corresponding matrix for noninteracting blobs ($v_{\alpha\beta}(r) = 0$), that is

$$\underline{S_0}(k) = \begin{pmatrix} 1 & \hat{s}_{AB}(k) \\ \hat{s}_{AB}(k) & 1 \end{pmatrix} \tag{7}$$

and $\underline{\hat{V}}(k)$ is the matrix of Fourier transforms (FT) $\hat{v}_{\alpha\beta}(k)$ of the blob−blob interaction potentials $v_{\alpha\beta}(r)$, then the RPA simply reads[39]

$$\underline{S}^{-1}(k) = \underline{S_0}^{-1}(k) + \rho\beta\underline{\hat{V}}(k) \tag{8}$$

In eq 7, $\hat{s}_{AB}(k)$ is the FT of the intramolecular CM−CM distribution function $s_{AB}(r)$,and $\beta = 1/k_BT$ in eq 8.

Equation 8 also applies to binary A−B mixtures, with $\underline{S_0}(k) = 1$, that is, $\hat{s}_{AB} \equiv 0$ in eq 7.

The resulting partial structure factors are of the generic form

$$S_{\alpha\beta}(k) = \frac{f_{\alpha\beta}(k,\rho)}{D_c(k,\rho)} \tag{9}$$

where

$$D_c(k,\rho) = 1 + \rho\beta[\hat{v}_{AA}(k) + \hat{v}_{BB}(k) - 2\hat{s}_{AB}(k)\hat{v}_{AB}(k)] + \rho^2\beta^2[\hat{v}_{AA}(k)\hat{v}_{BB}(k) - \hat{v}^2_{AB}(k)][1 - \hat{s}^2_{AB}(k)] \tag{10}$$

These expressions are identical to those obtained from the "reference interaction site model" (RISM) equations for dumbbells[40] with an RPA closure; the resulting explicit expressions for the $f_{\alpha\beta}(k, \rho)$ are given in ref 41. The three partial structure factors (eq 9) are shown in Figure 3 for the case $f = 0.6$ and several values of ρ/ρ^*, together with some MC data (cf. section V). A peak develops in all three structure factors around $q = kR_g \simeq 2$, the amplitude of which diverges for $\rho/\rho^* > 2$. The divergence occurs when the common denominator $D_c(k, \rho)$ of all three $S_{\alpha\beta}(k)$ goes to zero at a critical reduced wavenumber $q_c = k_cR_g$ beyond a critical reduced density ρ_c/ρ^*. For higher densities, the structure factors become unphysical (in particular $S_{AA}(k)$ and $S_{BB}(k)$ become negative), signaling an instability of the homogeneous solution of copolymers, and providing an estimate of the onset of clustering associated with microphase separation.

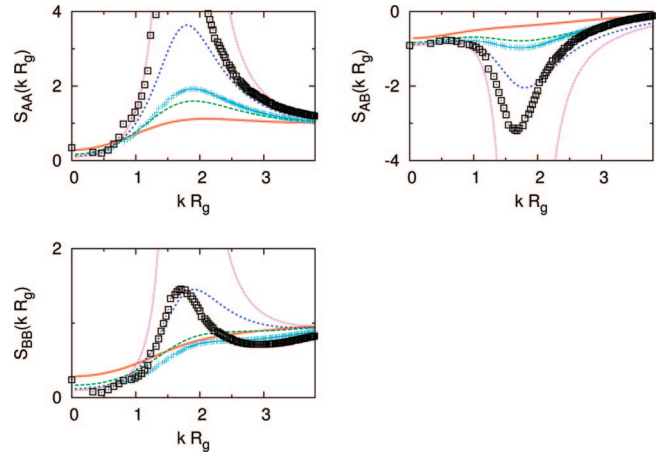

Figure 3. RPA predictions (eqs 9 and 10) for the partial structure factors $S_{\alpha\beta}$ as functions of the reduced wavenumbers kR_g for AB diblock copolymers with $f = 0.6$ in the soft dumbbell representation. The full curve, dashes, large dots, and small dots are for reduced densities $\rho/\rho^* = 0.5$, 1, 1.5, and 1.85 respectively, while the crosses and squares are MC data for $\rho/\rho^* = 2.5$ and 3.

TABLE 2: Critical Density ρ_c at which the RPA Structure Factors Diverge, Using the Diblock Copolymer Effective Potential Parameters (Diblock Copolymer Potentials DBP) and the Binary Mixture Effective Potential Parameters, Combined with the Diblock Tethering Potential (Binary Mixture Potentials BMP)[a]

f	DBP	BMP	cmc
1/5	25.0	12.57	$\rho/\rho^* > 7$
2/5	4.97	4.27	$4 < \rho/\rho^* < 4.5$
1/2	2.83	2.44	$3 < \rho/\rho^* < 3.5$
3/5	2.02	1.85	$2.5 < \rho/\rho^* < 3.$
4/5	1.65	1.13	$2 < \rho/\rho^* < 2.5$

[a] The MC estimates of the cmc are given in the right-hand column.

The MC data presented in the following sections show micelle formation at sufficiently high ρ/ρ^*, so that the divergence of the RPA structure factors may be interpreted as providing a rough estimate of the critical micellar concentration (cmc). The critical densities ρ_c/ρ^* are listed in Table 2.

In the case of a binary A−B mixture (i.e., setting $\hat{s}_{AB}(k) = 0$ in eq 10), $D_c(k, \rho)$ goes first to zero at $k = 0$ as ρ reaches a critical value ρ_c, that is, the three partial structure factors diverge at the origin, signaling a bulk (macroscopic) phase separation.

One immediately derives the osmotic compressibility from the $k \rightarrow 0$ limit of the partial structure factors (eq 9); integration of the latter over the copolymer density yields the osmotic pressure P, and further integration leads to the free energy and hence to the chemical potential within the RPA.

V. Clustering and Self-Assembly of Soft Dumbbells

We have carried out extensive MC simulations of systems of $N = 5000$ soft dumbbells interacting via the effective pair potentials discussed in section III within the NVT ensemble. Taking into account the guidelines provided by the RPA results of section IV, as well as our earlier results for the symmetric model ($f = (1/2)$),[28] we have explored the density range of $2 \leq \rho/\rho^* \leq 7$ for $f = 0.2$, 0.4, 0.6, and 0.8. Because the effective interactions are short-ranged, linked list tables were used to keep

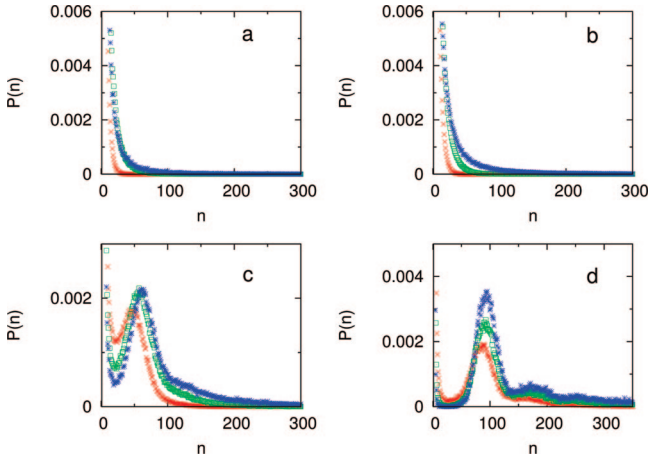

Figure 4. Cluster size distribution functions $P(n)$ for (f, ρ/ρ^*) pairs (a) (0.2, 4.), (b) (0.4, 3.5), (c) (0.6, 3.5), and (d) (0.8, 3.5). The $P(n)$ were calculated with three different values of the cuf-off distance $r_c/R_g = 0.7$ (crosses), 0.8 (squares), and 0.9 (stars) in the cluster criterion.

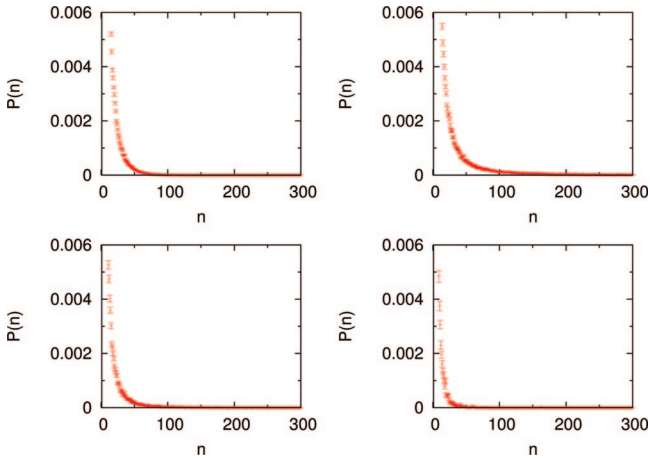

Figure 5. Cluster size distribution functions for $f = 0.2$ and $\rho/\rho^* = 4$, 5, 6, and 7; the cutoff $r_c = 0.8R_g$ has been used throughout. There is no sign of micellization even at the highest density.

track of close pairs of neighboring blobs. The standard Metropolis MC algorithm was used; the softness of the effective interactions allows the use of large trial moves and hence a very efficient sampling of configuration space. Clustering of copolymers is observed already at moderate densities. This is characterized by the cluster size distribution function $P(n)$, that is, the probability of finding a cluster of aggregation number n. A cluster is defined by the operational convention that all A blobs whose centers are situated within a distance r_c of any other A blob belong to the same cluster. The choice of r_c is somewhat arbitrary, but we observed that $P(n)$, averaged over a large number of copolymer configurations generated during the MC simulations, is rather insensitive to small variations of r_c around the value of $r_c = 0.8R_g$, as illustrated in Figure 4; this value of r_c was adopted in all subsequent calculations.

Results for $P(n)$ corresponding to the size ratios $f = 0.2$, 0.4, 0.6, and 0.8 and several densities are shown in Figures 5−8.

No clustering is observed for $f = 0.2$ up to the highest density considered here, in accordance with the RPA prediction of an instability of the homogeneous phase occurring at higher density (cf. Table 2). In the case where $f = 0.4$, clustering is seen to set in at $\rho/\rho^* \simeq 4.2$; at higher densities, a clear-cut bimodal distribution is observed, signaling the coexistence of clusters of mean aggregation number ≃100 with nearly isolated co-

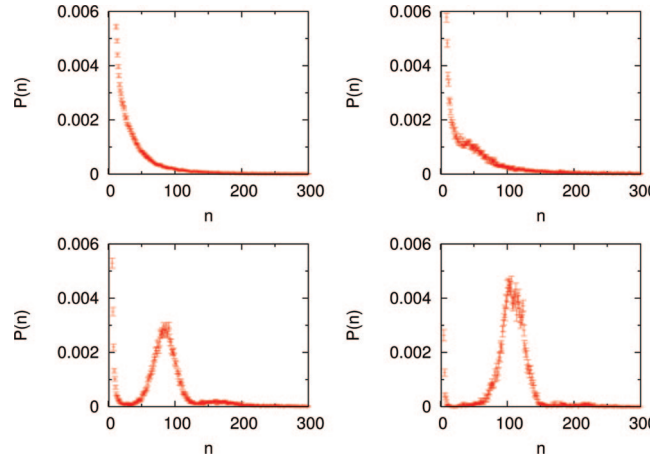

Figure 6. Same as Figure 5 but for $f = 0.4$ and $\rho/\rho^* = 4.5$, 5, 6, and 7.

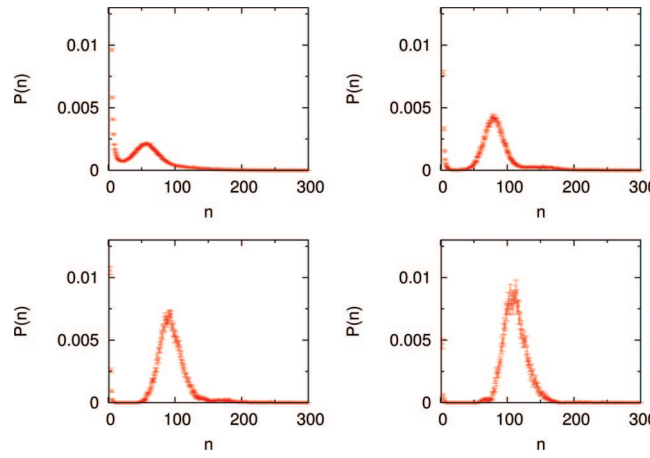

Figure 7. Same as Figure 5 but for $f = 0.6$ and $\rho/\rho^* = 3.5$, 4, 4.5, and 5.

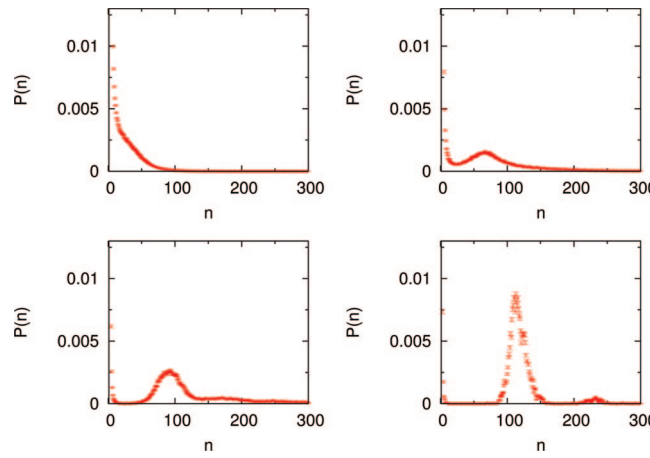

Figure 8. Same as Figure 5 but for $f = 0.8$ and $\rho/\rho^* = 2.5$, 3, 3.5, and 4.

polymers. Similar trends are observed for $f = 0.6$ and 0.8 with clusters forming at even lower densities, which gradually increase at the expense of the number of remaining isolated copolymers. Inspection of the structure of the clusters shows that they are quasi-spherical micelles, as discussed in the following section. Within the present ISS model, micellization is seen to set in at a relatively high copolymer concentration, which makes a clear-cut definition of the cmc rather delicate. We have adopted the following operational definition:[14] if n_0 is the aggregation number corresponding to the minimum in the

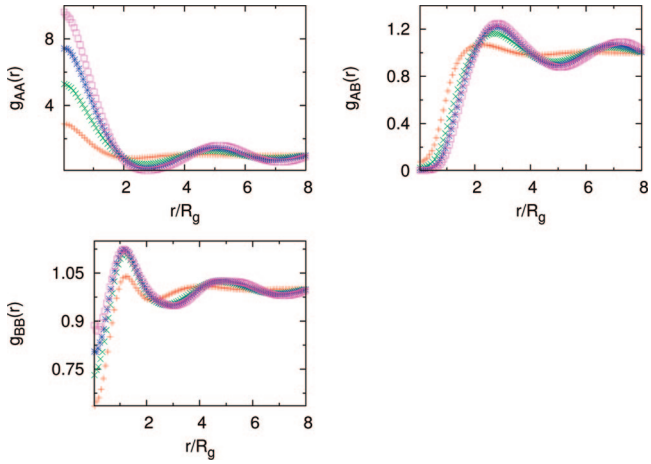

Figure 9. Partial blob−blob pair distribution functions $g_{\alpha\beta}(r)$ versus reduced CM−CM distance r/R_g for $f = 0.6$ and $\rho/\rho^* = 3$ (pluses), 4.5 (crosses), 5 (stars), and 6 (squares).

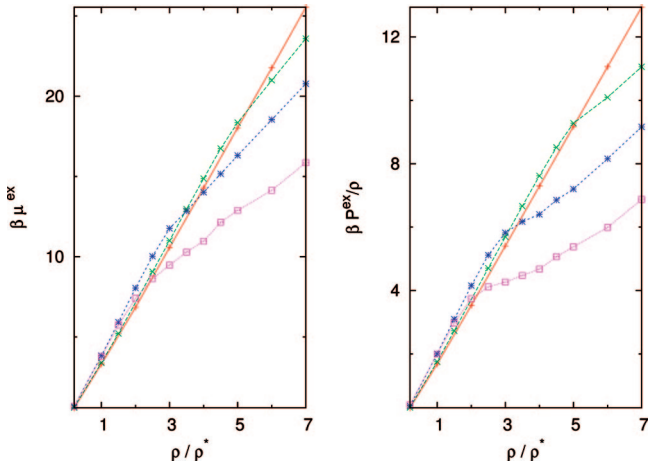

Figure 10. Reduced excess (nonideal) chemical potential $\beta\mu^{ex}$ (left frame), and osmotic equation of state $\beta P^{ex}/\rho$ (right frame) versus reduced copolymer density ρ/ρ^* for $f = 0.2$ (pluses), 0.4 (crosses), 0.6 (stars), and 0.8 (squares). The corresponding slopes of the RPA prediction (eq 15) are $\zeta = 3.48$ for $f = 0.2$, 4.20 for $f = 0.4$, 4.68 for $f = 0.6$, and 4.7 for $f = 0.8$.

bimodal distribution $P(n)$, then, upon increasing the polymer density, the cmc is reached when

$$\sum_{i=1}^{n_0} iP(i) = \sum_{j=n_0+1}^{N} jP(j) \tag{11}$$

The resulting cmc values are listed in Table 2 and are seen to correlate with the trend predicted by the RPA.

The onset of clustering is also apparent in the partial intermolecular blob−blob pair distribution functions $g_{\alpha\beta}(r)$, examples of which are shown in Figure 9. Strong oscillations build up at higher densities, signaling the spatial inhomogeneity associated with micellization. Upon Fourier transformation, yielding the partial structure factors $S_{\alpha\beta}(k)$, these oscillations give rise to the pronounced peaks shown in Figure 3, which eventually diverge near the cmc.

We have also looked for a possible thermodynamic signature of microphase separation associated with micellization. Obviously, one does not expect the singularities associated with bulk phase separation, but some rapid continuous changes may be apparent near the cmc. The chemical potential μ of the

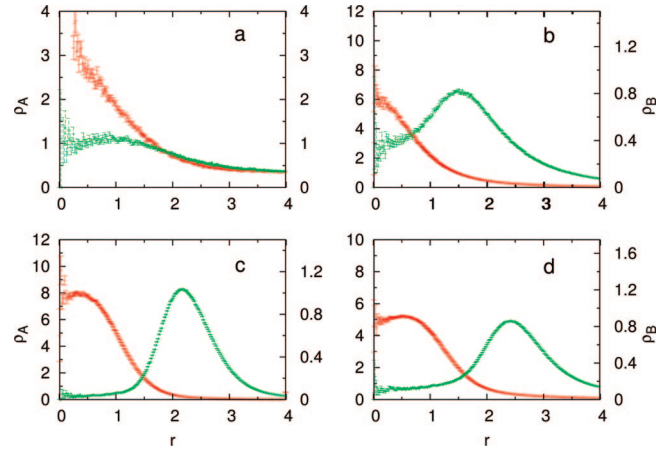

Figure 11. Radial densities ρ_A (left-hand curve and scale in each frame) and ρ_B (right-hand) as a function of the reduced distances $r = r_{CM}/R_g$ of the CMs of A and B blobs from the micelle CM for (a) $f = 0.2$, $\rho/\rho^* = 6$.; (b) (0.4, 5); (c) (0.6, 4) and (d) (0.8, 3.5). Note that the case where $f = 0.2$ is irrelevant because of the absence of micellization.

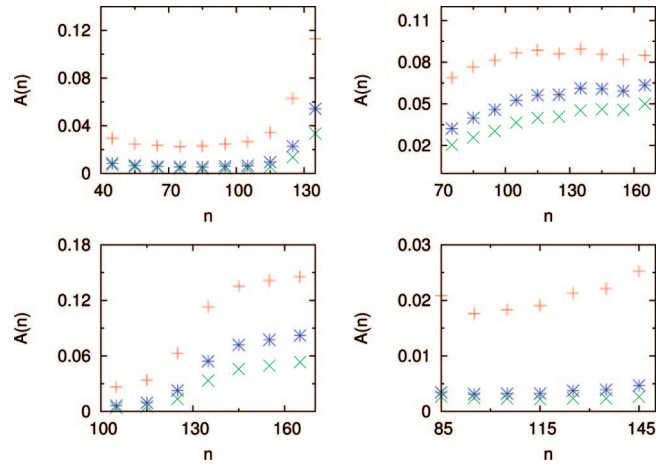

Figure 12. The three asphericity ratios, core (crosses), corona (pluses), and total (stars), for the micelles as defined in eq 20. The four panels shows the cases ($f = 0.4$, $\rho/\rho^* = 6$), ($f = 0.6$, $\rho/\rho^* = 5$), ($f = 0.6$, $\rho/\rho^* = 6$), and ($f = 0.8$, $\rho/\rho^* = 4$).

copolymers is easily estimated by the Widom insertion method,[39,42] based on the exact relation for the excess (nonideal) part

$$\beta\mu_{ex} = -[\ln(I_1) - \ln(I_2)] \tag{12}$$

where

$$I_1 = \iint d\vec{r}^A d\vec{r}^B \exp\{-\beta\Psi_{AB}(|\vec{r}^A - \vec{r}^B|)\}\langle\exp\{-\beta\Delta V\}\rangle_N$$
$$I_2 = \iint d\vec{r}^A d\vec{r}^B \exp\{-\beta\Psi_{AB}(|\vec{r}^A - \vec{r}^B|)\} \tag{13}$$

$$\Delta V(\vec{r}^A, \vec{r}^B) = \sum_{i=1}^{N}\sum_{\alpha\beta} v_{\alpha\beta}(|\vec{r}^\alpha - \vec{r}_i^\beta|) \tag{14}$$

The statistical average in eq 14 is taken over a canonical ensemble of N copolymers. The $\vec{r}^A$ and $\vec{r}^B$ are the positions of the centers of the additional A and B blobs which are inserted into a system of N copolymers.

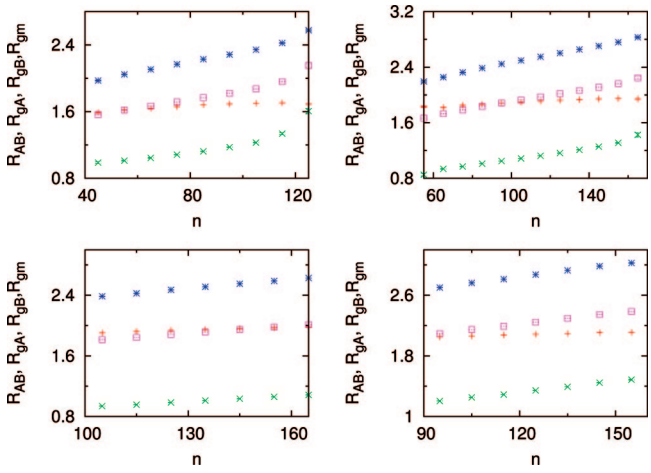

Figure 13. Bond length R_{AB} of AB dumbbells (plus signs), radius of gyration R_{gA} of the micellar core (crosses), radius of gyration of the corona R_{gB} (stars), and total micellar radius of gyration R_{gm} (squares) as functions of the aggregation number n of micelles for $(f, \rho/\rho^*) = (0.4, 6)$; (0.6, 5); (0.6, 6); and (0.8, 4) (from top left to bottom right); all lengths are in units of the zero-density copolymer radius of gyration R_g.

The Widom method is particularly efficient in MC simulations because of the softness of the blob−blob interactions, which allows a high acceptance rate of the attempted insertions. The μ_{ex} is easily calculated within the RPA, as explained in section IV, and turns out to be a linear function of the density:

$$\beta\mu_{ex}^{RPA} = \zeta\frac{\rho}{\rho^*} \tag{15}$$

$$\zeta = \frac{3}{4\pi}\sum_{\alpha}\sum_{\beta}\left(A_{\alpha\beta}\frac{\pi}{a_{\alpha\beta}}\right)^{3/2} \tag{16}$$

MC estimates of the osmotic equation of state (e.o.s) $Z = \beta P/\rho$ are calculated from the standard virial expression

$$\frac{\beta P}{\rho} = 2 - \frac{\beta}{3N}\sum_{\alpha}\sum_{\beta}\langle\sum_{i}\sum_{j>i}\upsilon'_{\alpha\beta}(|\vec{r}_i^{\,\alpha} - \vec{r}_j^{\,\beta}|)|\vec{r}_i^{\,\alpha} - \vec{r}_j^{\,\beta}|\rangle - \frac{\beta}{3N}\langle\sum_{i}\Psi'_{AB}(|\vec{r}_i^{\,A} - \vec{r}_i^{\,B}|)|\vec{r}_i^{\,A} - \vec{r}_i^{\,B}|\rangle \tag{17}$$

where the prime denotes a derivative with respect to the argument.

The RPA leads to the linear expression

$$\frac{\beta P}{\rho} = 1 + \frac{\zeta}{2}\frac{\rho}{\rho^*} \tag{18}$$

MC results for $\beta\mu_{ex}$ and $(\beta P_{ex})/\rho$ are plotted in Figure 10 as functions of ρ/ρ^* for $f = 0.2$, 0.4, 0.6, and 0.8. The variation is practically linear in the case where $f = 0.2$, with slopes comparable to the RPA predictions (eqs 15 and 18). For larger size ratios f, there is clear evidence of a break in the slope at a density ρ/ρ^* which decreases as f increases; these crossover densities correlate well with the estimated values of the cmc listed in Table 2. As expected, the osmotic pressure rises less rapidly with density once micellization sets in.

VI. Internal Structure of Micelles

Once large clusters and micelles have been identified as explained in the previous section, the MC code determines, for each micelle, its CM, radius of gyration R_{gm} as well as the A−B bond length R_{AB} and the radial blob densities $\rho_A(r)$ and $\rho_B(r)$ as functions of the distance r of their CMs from the micelle CM. Examples for $f = 0.4$, 0.6, and 0.8, close to their estimated cmc's, are shown in Figure 11.

In all three cases, the A blobs are seen to be confined to a core ($\rho_A(r) \simeq 0$ for $r \geq 2R_g$), while the B blobs form an external corona. The interface between the core and corona is relatively sharp, as expected from the repulsion between A and B blobs. The variation of the radii of gyration and that of R_{AB} (the bond length of the copolymers) with n is plotted in Figure 13. As expected, the radii of gyration and the bond length increase with aggregation number, that is, the copolymers are more stretched when n increases.

The average shape of the micelles is conveniently characterized by asphericity parameter A defined as follows.[43] We first introduce the gyration tensor of a micelle of n effective dumbbells

$$g_{\alpha\beta}(n) = \frac{1}{2n}\langle\sum_{\gamma=A,B}\sum_{k=1}^{n}(r_{k\alpha}^{\gamma} - r_{CM,\alpha})(r_{k\beta}^{\gamma} - r_{CM,\beta})\rangle \tag{19}$$

Core and corona contributions to the tensor can be separated by restricting the sum over A and B to one of the two blobs; $r_{CM,\alpha}$ are the coordinates of the micelle CM.

If $g_a \leq g_b \leq g_c$ are the three eigenvalues of this tensor, the latter will be equal for a spherical micelle. The asphericity $A(n)$, as a funcion of the number of particles per cluster, is then defined as

$$A(n) = \frac{(g_a(n) - g_b(n))^2 + (g_a(n) - g_c(n))^2 + (g_c(n) - g_b(n))^2}{2(g_a(n) + g_b(n) + g_c(n))^2} \tag{20}$$

For a spherical micelle, $A(n) = 0$, while for a cylindrical micelle, $A(n) = 1$. The variation of $A(n)$ with aggregation number, as estimated from our MC simulations for a few values of f and ρ/ρ^*, is illustrated in Figure 12, which features the values of $A(n)$ for the micellar core, the corona, and the complete micelle. The asphericity is seen to be small in all cases. The significant increase of $A(n)$ at large n in some cases is due to the fact that some micelles nearly touch and are seen as nonspherical fused micelle pairs within the convention adopted to define clusters.

There has been some debate about the copolymer length dependence of the micelle size, as predicted by self-consistent field theory and by computer simulation.[8,43] In the highly concentrated solution or melt regimes considered in these studies, where the chains obey Gaussian statistics, the micelle radius scales, to leading order, like $L^{1/2}$. On the other hand, the present work deals with the semidilute regime, where Gaussian statistics no longer apply, so that a direct comparison with previous predictions is not possible. In the present soft dumbbell representation of the copolymers, the micelle size is controlled by the effective blob−blob interactions in eqs 5 and 6. The only length scale in the latter is the radius of gyration R_g of an isolated copolymer, so that, for a given copolymer concentration, the

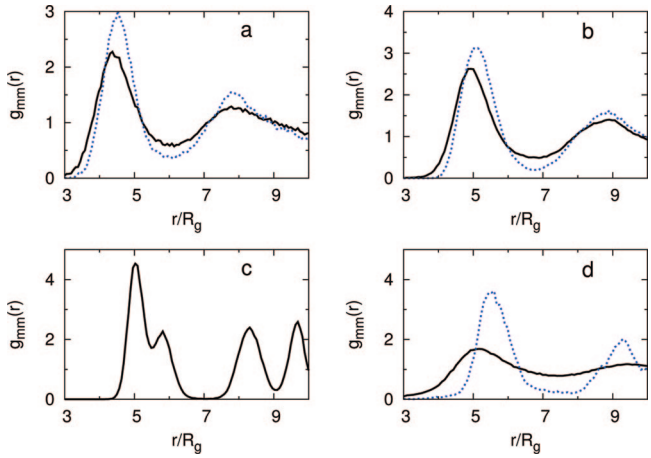

Figure 14. Pair distribution functions $g_{mm}(r)$ of the micelle CMs versus (reduced) CM−CM distance r/R_g; (a) $f = 0.4$, $\rho/\rho^* = 6$ and 7; (b) $f = 0.6$, $\rho/\rho^* = 4$ and 5; (c) $f = 0.6$, $\rho/\rho^* = 6$ (BCC crystal of micelles); (d) $f = 0.8$, $\rho/\rho^* = 3$ and 4.

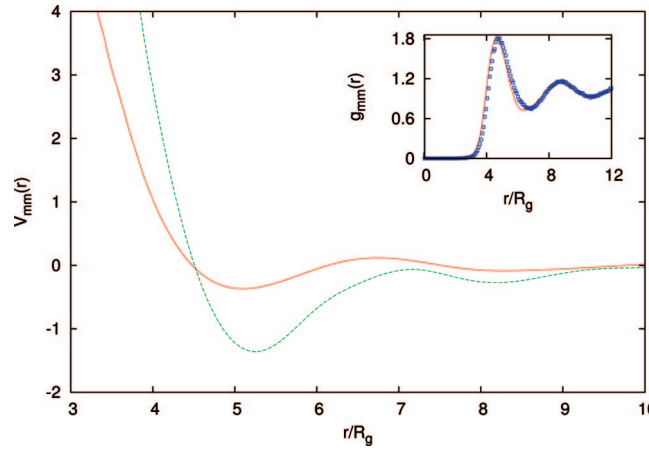

Figure 15. Effective pair potentials $v_{mm}(r)$ between the micelle CMs versus r/R_g for $f = 0.6$ and $\rho/\rho^* = 3.5$ (full curve) and 4. (dashed curve). The inset shows the pair distribution function $g_{mm}(r)$ for $\rho/\rho^* = 3.5$ computed from the effective potential $v_{mm}(r)$ by a MC simulation (full line) compared to the original MC data based on the dumbbell representation of individual copolymers (squares).

micelle size is proportional to R_g, which no longer scales like $L^{1/2}$ in the semidilute regime.

VII. Micellar Pair Structure

Beyond the cmc, once micelles have formed, they remain stable over the total duration of the MC runs (typically 10^4 trial moves per copolymer), although their aggregation number n fluctuates due to exchanges of copolymers between micelles or between micelles and "free" copolymers, giving rise to the size polydispersity evident in Figures 6−8. Microphase separation results in an inhomogeneous solution of "free" copolymers coexisting with micelles containing typically 10^2 copolymers each; the fraction of "free" copolymers drops rapidly beyond the cmc, and the initial copolymer solution turns into a suspension of quasi-spherical micelles which grow in size (i.e., increase with increasing copolymer density ρ/ρ^*) until all free copolymers have been aggregated.

It is worth noting that the exchange of copolymers between micelles is greatly facilitated by the soft dumbbell representation, compared to a full monomer-level representation, because copolymers no longer have to disentangle during the exchange process, while the energy barrier to be overcome by an effective dumbbell leaving or entering a micelle is only on the order of a few k_BT due to the interaction with surrounding dumbbells.

Going one step further in the systematic coarse-graining procedure, we have determined the micelle−micelle pair distribution function (p.d.f.) of the distance between micelle CMs, averaged over all pairs of micelles, irrespective of their aggregation number n. Examples are shown in Figure 14 for copolymer densities close to and above the cmc.

For all three values of f, the p.d.f. at the lower density is typical of that of a simple dense atomic fluid exhibiting short-range order. The pair structure is seen to be more sharply defined at the higher density, with hints of long-range order characteristic of a crystalline structure; a similar observation was already made in our earlier work on a symmetric ($f = 0.5$) diblock copolymer.[28] At the highest density ($\rho/\rho^* = 6$), in the case $f = 0.6$, the positions of the peaks in the p.d.f. clearly point to a bcc crystal. The long-range crystalline order is confirmed in that case by the computed static structure factor, which exhibits sharp Bragg peaks at the expected wave vectors. However, in other cases, the determination of the crystal structure proves more difficult, for a number of reasons. First, the number of micelles formed from a system of $N = 5000$ dumbbells is on the order of 50. Apart from being relatively small, the number of spontaneously formed micelles is not, in general, compatible with the periodic boundary conditions for any given crystal structure. Moreover the size polydispersity of the micelles will tend to prevent crystallization and favor disordered amorphous structure at high density. Our preliminary investigations of the high-density micellar phase suggest the formation of either defective crystals or completely amorphous structures, depending on the density, initial conditions, and the size ratio f. More work along these lines is under way and will be published elsewhere. Returning to the disordered (fluid) micellar phase just above the cmc, we have determined the effective pair potential $v_{mm}(r)$ between micelles by inverting the measured p.d.f.'s using the hypernetted chain (HNC) closure of liquid state theory,[28,44] namely

$$v_{mm}(r) = k_BT\{g_{mm}(r) - 1 - c_{mm}(r) - \ln[g_{mm}(r)]\} \quad (21)$$

where $c_{mm}(r)$ is the direct correlation function related to $g_{mm}(r)$ by the Orstein−Zernike relation.[44] The numerical inversion requires special care because $g_{mm}(r)$ is vanishingly small for $r/R_g \lesssim 3$, as shown in Figure 14, signaling a strong, effective micelle−micelle repulsion at short distances. Moreover, in the presence of strong micelle−micelle correlations, near crystallization, the inversion is particularly cumbersome because of the small number of micelles present in our systems (roughly 50). In these situations (see, for instance, panel a of Figure 14), the oscillations in the $g_{mm}(r)$ are still quite pronounced at the edge of the box, which makes it difficult to consistently extrapolate the behavior at large distances with a model fitted on the short distance data. We have found it more convenient to assume a polynomial behavior for $S_{mm}(k)$ at small k's and make a fit combining data from $g_{mm}(r)$ and $S_{mm}(k)$. Full details of the inversion procedure will be reported in a forthcoming publication.[45] The resulting $v_{mm}(r)$ for $f = 0.6$ are shown in Figure 15. The effective potentials exhibit a soft core repulsion, with an amplitude at full overlap ($r = 0$) of about $20k_BT$. It is interesting to note that in the limit of vanishing core size (i.e., of very short A blocks), the micelles would be similar to star polymers, with arms provided by the SAW B blocks; the effective repulsion between star polymers is known to be

logarithmic.[46,47] The attractive tail in $v_{mm}(r)$ could be due to the familiar depletion effect,[39] the role of the depletant being played by the "free" copolymers in the solution. This behavior is reminiscent of the attraction between star polymers induced by shorter linear polymers.[48]

The effective pair potentials shown in Figure 15 are seen to be rather sensitive to the copolymer density. The rapid change with ρ reflects the increase in mean aggregation number (cf. Figure 7) and the concomitant increase in micelle size. The reduced micelle density $\rho_m^* = \rho_m(2R_{gm})^3$ is 0.49 for $\rho/\rho^* = 3.5$ and 0.61 for $\rho/\rho^* = 4$. The deepening of the attractive well in $v_{mm}(r)$ as ρ/ρ^* increases is somewhat counterintuitive within the standard Asakura−Oosawa model of mixtures of hard-sphere colloids and nonadsorbing ideal polymers, which predicts a linear increase of the depletion-induced attraction with polymer concentration.[39] In the present situation, where micelles coexist with "free" copolymers, the concentration of the latter decreases with increasing ρ/ρ^*, so that one would be tempted to expect a reduction in depletion-induced attraction. The opposite behavior observed here may be due to two factors, the micelles are fluctuating soft rather than hard particles and the depletant is constantly exchanged between micelles, leading to strong fluctuations in the local number of "free" copolymers.

We have checked the consistency of the inversion procedure by comparing the p.d.f. $g_{mm}(r)$ obtained from the dumbbell simulations with that computed using the effective micelle−micelle potential; an example of this comparison shown in the inset of Figure 15 is conclusive and validates the relevance of the $v_{mm}(r)$ shown in Figure 15.

VIII. Discussion and Conclusion

In this paper, we have extended a systematic three-step coarse-graining procedure for an efficient multiscale description of diblock copolymer self-assembly in a selective solvent, first introduced in our earlier work,[28,33] to the case of ISS diblocks of arbitrary size ratio f. In a first step, the initial full monomer representation of AB diblock copolymers is mapped onto a system of "soft dumbbells", where the two blocks are represented by effective segments or "blobs" which interact via the effective pair potentials (eqs 5 and 6). These potentials are determined by a rigorous inversion procedure of the blob−blob p.d.f's generated in MC simulations of an isolated copolymer or a pair of isolated blobs, that is, in the zero-density limit. Under the assumption that these effective interactions are independent of copolymer density, the second step of the coarse-graining strategy is to carry out MC simulations of the dumbbell model over a range of densities well into the semidilute regime ($\rho > \rho^*$) to explore the clustering and eventual microphase separation associated with the formation of stable micelles and ultimately the disorder−order transition of these micelles.

The final step is to extract the effective pair potentials between these micelles by inverting the p.d.f's of the micelle CMs. These effective micelle−micelle potentials will be used in a subsequent paper for a systematic investigation of the disorder−order transition and of the structure of the ordered phase.

The key finding of our work is that the ISS model systematically leads to the formation of spherical micelles, irrespective of size ratio f. The cmc is found to drop rapidly as f increases; since there is obviously no microphase separation in the limits of $f \rightarrow 0$ and $f \rightarrow 1$ corresponding to B and A homopolymers, respectively, the cmc must go through a minimum for some intermediate value of f, close to $f = 0.8$ according to the MC estimates. It is gratifying to find that the variation of the cmc with f correlates well with the stability limit of the homogeneous copolymer phase predicted by the RPA (cf. Table 1). The micellar phase appears to be the only stable microphase of the ISS model. The cylindrical phase was found to be systematically unstable. Starting from an initial configuration of an hexagonal array of parallel cylinders with A cores and B coronae, prepared by applying an external field, we found that the imposed structure rapidly broke up upon removal of the external field in MC simulations. Simple entropic considerations show that the BA AB lamellar phase is unlikely to be stable against a breakup into micelles.

The exclusive formation of disordered and ordered phases of spherical micelles is not an artifact of the soft dumbbell representation of the copolymers but is an intrinsic feature of the underlying microscopic ISS model which mimics diblock copolymers in a highly selective solvent. Selective swelling favors phases with strong curvatures in the microphase-separated state, and hence, the formation of spherical micelles, and their crystallization, pre-empts the formation of any other phase in the semidilute regime under consideration here, as illustrated by the detailed experimental phase diagrams of Lodge et al.[11] The latter data also show that micelles do not form for small size ratios f, in qualitative agreement with the predictions of the present simulations (cf. Figure 5). It is worth recalling at this point that a lamellar phase was obtained in our earlier simulations of the related ISI diblock copolymer model,[33] thus confirming that the dumbbell representation in itself does not favor spherical micelles.

Before concluding, it is important to discuss the consistency of our coarse-graining procedure. The self-assembly scenario of the soft dumbbell model predicted by MC simulations may be considered to be "exact" within numerical uncertainties, provided finite size effects and ergodicity problems are overcome by simulating sufficiently large samples with sufficient statistics (i.e., over a sufficiently large number of MC moves). Thus, our findings are expected to be valid for the coarse-grained soft dumbbell model. There is, however, an inconsistency in the first step of the coarse-graining procedure, that is, in the link between the original, atomistic ISS model and its soft dumbbell representation, due to the fact that we have used the low-density limit of the effective blob−blob pair potentials, while the MC simulations based on these potentials were carried out in the semidilute regime ($\rho/\rho^* > 1$), where clustering and microphase separation take place. This approximation should not lead to qualitatively wrong predictions, in view of the fact that, at least in the single blob representation of interacting homopolymers, the effective blob−blob potential has been shown to be only moderately density-dependent;[15] contrary to the case of homopolymers, there is, however, no obvious way of inverting the copolymer pair structure at finite density to extract reliable density-dependent pair potentials. This difficulty can be circumvented by switching to a multiblob representation of the A and B blocks of the copolymers, similar to that recently put forward for homopolymers.[17] Replacing a single blob by n blobs, each associated with L_α/n (α = A or B) monomers, ensures that the blob overlap density ρ_b^* is larger than the initial overlap density ρ^* (by a factor $n^{3\nu-1} \simeq n^{4/5}$ [17]), so that the use of the low-density effective blob−blob interactions is justified, as long as $\rho_b/\rho_b^* < 1$. Work on the multiblob representation of copolymer solutions is under way.

An obvious limitation of the ISS model is that it is athermal, while experimental copolymer phase diagrams span the whole temperature−density plane.[2,11−13] To take into account solvent selectivity in a systematic way, one must introduce an energy scale in the atomistic model. The simplest generalization of the present ISS model is to introduce nearest-neighbor monomer

attractions. In other words, both the A and B blocks are modeled as self- and mutually avoiding walks (SAW) and the attractive energies $-\epsilon_{AA}$, $-\epsilon_{AB}$, and $-\epsilon_{BB}$ are introduced between nonbonded, adjacent A−A, A−B, and B−B monomer pairs. Solvent selectivity is thus controlled by the choice of these attractive energies. The ISS model investigated in this paper amounts to choosing $\epsilon_{BB} = \epsilon_{AB} = 0$ and, roughly speaking, choosing ϵ_{AA} such that the A blocks are under θ conditions, so that they behave, at least approximately, like ideal (Gaussian) chains. The coarse-graining procedure used in the present paper is easily applicable to the more realistic model described above, and work along these lines is in progress.

Acknowledgment. The authors thank Ivan Coluzza for help with the numerical work and Wolfgang Götze for a useful suggestions. B.C. would like to thank John Molina for useful discussions. B.C. is supported by an EU Marie Curie Fellowship. C.P. thanks Schlumberger Cambridge Research and the Royal Society of London for support during visits to Cambridge, while J.P.H. is grateful for support from Università di Roma "La Sapienza" during a visit to Rome.

Appendix

A: Inversion of Site−Site Pair Distribution Functions. In this appendix, we outline the numerical procedure used to extract the site−site effective pair potentials $v_{\alpha\beta}(r)$ from the knowledge of the site−site pair distribution functions $s_{AB}(r)$ and $g_{\alpha\beta}(r)$ in the zero-density limit.

The inversion procedure is based on the exact set of equations first derived by Ladanyi and Chandler[34] and recalled in ref 33. In terms of cluster diagrams based on the intramolecular pair distribution function $s_{AB}(r)$ and on the Mayer functions $f_{\alpha\beta}(r)$ associated with the site−site pair potentials, these equations prescribe that, for two-site molecules, the intermolecular site−site pair correlation functions $h_{\alpha\beta}(r) = g_{\alpha\beta}(r) - 1$ are sums of 15 diagrams.[34] Thirteen of them are reducible to products and convolutions of real space functions. Therefore, for a given set of Mayer functions, they are easily handled using fast Fourier transform techniques. The last remaining two diagrams are more problematic since they have the topology of bridge diagrams which cannot be resolved by simple Fourier transforms. They can be computed using the method of Legendre transform in its discrete, orthogonal version proposed by Attard.[49]

Using these simple numerical methods for the evaluation of individual diagrams, the actual computation of the site−site effective pair potentials mainly proceeds via a Picard iteration scheme. The Ladanyi−Chandler equations are first rewritten in the form of fixed point equations for the Mayer functions

$$f_{\alpha\beta}(r) = F_{\alpha\beta}[s_{AB}, h_{\gamma\delta}, f_{\gamma\delta}](r) \quad \text{(A1)}$$

where s_{AB} and the $h_{\gamma\delta}$'s are the correlation functions obtained from the full monomer MC simulations. Different expressions have been considered for the $F_{\alpha\beta}$'s, which all seemed to be equivalent in terms of convergence and accuracy. Then, starting from an initial guess $f^{(0)}_{\alpha\beta}(r)$, one loops through

$$f^{(i+1)}_{\alpha\beta}(r) = (1 - x)F_{\alpha\beta}[s_{AB}, h_{\gamma\delta}, f^{(i)}_{\gamma\delta}](r) + x f^{(i)}_{\alpha\beta}(r) \quad \text{(A2)}$$

until convergence is achieved. The x is a mixing parameter close to 1 (typically, between 0.9 and 0.99) tuned to improve the stability of the iterative scheme.

Once the stable Mayer functions are obtained, it is a trivial step to extract the potentials from them.

References and Notes

(1) Safran, S. A. *Statistical Thermodynamics of Surfaces, Interfaces and Membranes*; Addison-Wesley: Reading, MA, 1994.
(2) Hamley, I. W. *Block Copolymers in Solution*; Wiley: Chichester, U.K., 2005.
(3) Leibler, L. *Macromolecules* **1980**, *13*, 1602.
(4) Matsen, M. W.; Schick, M. *Phys. Rev. Lett.* **1994**, *72*, 2660.
(5) Ohta, T.; Kawasaki, K. *Macromolecules* **1986**, *18*, 2621.
(6) Fredrickson, G. H.; Helfand, E. *J. Chem. Phys.* **1987**, *87*, 697.
(7) Zhulina, E. B.; Adam, M.; La Rue, J.; Sheiko, S. S.; Rubinstein, M. *Macromolecules* **2005**, *38*, 5330.
(8) Milchev, A.; Bhattacharya, A.; Binder, K. *Macromolecules* **2001**, *34*, 1881.
(9) Termonia, V. *J. Polym. Sci., Part B: Polym. Phys.* **2002**, *40*, 890.
(10) Wijmans, C. M.; Eiser, E.; Frenkel, D. *J. Chem. Phys.* **2004**, *120*, 5839.
(11) Lodge, T. P.; Bang, J.; Li, Z.; Hillinger, M. H.; Talmon, Y. *Faraday Discuss.* **2005**, *128*, 1.
(12) Lodge, T. P.; Pudil, B.; Hanley, K. J. *Macromolecules* **2002**, *35*, 4707.
(13) Park, M. J.; Char, K.; Bang, J.; Lodge, T. P. *Macromolecules* **2005**, *38*, 2449.
(14) Bolhuis, P. G.; Frenkel, D. *Physica A* **1997**, *244*, 45.
(15) Bolhuis, P. G.; Louis, A. A.; Hansen, J.-P.; Meijer, E. J. *J. Chem. Phys.* **2001**, *114*, 4296.
(16) Krakoviack, V.; Hansen, J.-P.; Louis, A. A. *Phys. Rev. E* **2003**, *67*, 041801.
(17) Pierleoni, C.; Capone, B.; Hansen, J. P. *J. Chem. Phys.* **2007**, *127*, 171102.
(18) Bolhuis, P. G.; Louis, A. A.; Hansen, J.-P. *Phys. Rev. Lett.* **2002**, *89*, 128302.
(19) Pelissetto, A.; Hansen, J.-P. *Macromolecules* **2006**, *39*, 9571.
(20) Flory, P. J.; Krigbaum, W. R. *J. Chem. Phys.* **1950**, *18*, 1086.
(21) Grosberg, A. V.; Khalatur, P. G.; Khoklov, A. R. *Mater. Chem. Phys.* **1982**, *3*, 709.
(22) Dautenhahn, J.; Hall, C. K. *Macromolecules* **1994**, *27*, 5399.
(23) Krakoviack, V.; Rotenberg, B.; Hansen, J.-P. *J. Phys. Chem. B* **2004**, *108*, 6697.
(24) Sambriski, E. J.; Guenza, M. G. *Phys. Rev. E* **2007**, *76*, 051801.
(25) Eurich, F.; Karatchentsev, A.; Baschnagel, J.; Dieterich, W.; Maass, P. *J. Chem. Phys.* **2007**, *127*, 134905.
(26) Eurich, F.; Maass, P. *J. Chem. Phys.* **2001**, *114*, 7655.
(27) Murat, M.; Kremer, K. *J. Chem. Phys.* **1998**, *108*, 4340.
(28) Pierleoni, C.; Addison, C.; Hansen, J.-P.; Krakoviack, V. *Phys. Rev. Lett.* **2006**, *96*, 128302.
(29) Pelissetto, A.; Vicari, E. *Phys. Rep.* **2002**, *368*, 546.
(30) de Gennes, P. G. *Scaling Concepts in Polymer Physics*; Cornell University Press: Ithica, NY, 1979.
(31) Louis, A. A.; Bolhuis, P. G.; Hansen, J.-P. *Phys. Rev. E* **2000**, *62*, 7961.
(32) Addison, C. I.; Artola, P. A.; Hansen, J.-P.; Louis, A. A. *J. Phys. Chem. B* **2006**, *110*, 3661.
(33) Addison, C. I.; Hansen, J.-P.; Krakoviack, V.; Louis, A. A. *Mol. Phys.* **2005**, *103*, 3045.
(34) Ladanyi, B. M.; Chandler, D. *J. Chem. Phys.* **1975**, *62*, 4308.
(35) Pelissetto, A.; Hansen, J.-P. *J. Chem. Phys.* **2005**, *112*, 134904.
(36) Likos, C. N.; Lang, A. M. W.; Löwen, H. *Phys. Rev. E* **2001**, *63*, 031206.
(37) Mladek, B. M.; Gottwald, D.; Kahl, G.; Newmann, M.; Likos, C. N. *Phys. Rev. Lett.* **2006**, *96*, 045701.
(38) Likos, C. N.; Mladek, B. M.; Gottwald, D.; Kahl, G. *J. Chem. Phys.* **2007**, *126*, 224502.
(39) Barrat, J.-L.; Hansen, J.-P. *Basic Concepts for Simple and Complex Liquids*; Cambridge University Press; New York, 2003.
(40) Chandler, D. *Stud. Stat. Mech.* **1982**, *8*, 275.
(41) Hansen, J.-P.; Pearson, C. *Mol. Phys.* **2006**, *104*, 3389.
(42) Widom, B. *J. Chem. Phys.* **1963**, *39*, 2802.
(43) Cavallo, A.; Müller, M.; Binder, K. *Macromolecules* **2006**, *39*, 9539.
(44) Hansen, J.-P.; Mc Donald, I. R. *Theory of Simple Liquids*, 3rd ed.; Academic Press: Amsterdam, The Netherlands, 2006.
(45) Molina, J.; et al. To be published.
(46) Pincus, P.; Witten, T. *Europhys. Lett.* **1987**, *3*, 315.
(47) Likos, C. N. *Phys. Rep.* **2001**, *348*, 267.
(48) Mayer, C.; Likos, C. N. *Macromolecules* **2007**, *40*, 1196.
(49) Attard, P. *J. Chem. Phys.* **1989**, *91*, 3072.

JP805946Z